Springer

Journal of Mechanical Science and Technology 23 (2009) 3271~3280

Journal of Mechanical Science and Technology

www.springerlink.com/content/1738-494x
DOI 10.1007/s12206-009-0920-4

Controlled canard configuration study for a solid rocket motor based unmanned air vehicle †

Xie Kan[1,*], Liu Yu[1], and Xin Jianren[2]

[1]*Faculty 403, Beijing University of Aeronautics and Astronautics, Beijing 100191, China*
[2]*Department 2, China Academy of Aerospace Aerodynamics (CAAA), Beijing 100191, China*

(Manuscript Received February 23, 2009; Revised August 13, 2009; Accepted August 13, 2009)

Abstract

This paper presents an aerodynamic study for a target unmanned air vehicle with controlled canard, at cruise Mach number between 0.7 and 0.85, using a solid rocket motor as power. The results of semi-empirical method (DATCOM), computational fluid dynamics (CFD) were compared with wind tunnel tests to evaluate perdition accuracy. Here DATCOM shows big discrepancy in pitching-moment coefficient; the CFD estimation of static aerodynamic force and moment agree well with wind tunnel data. An analysis was focused on the longitudinal data for complicated controlled canard-elements interactions and canard vortex behavior. The canard vortex interaction with tail wing of initial configuration concept with a thick canard (NACA0012) and the final improved configuration with a thin canard (NACA0007) were reviewed. It is proved that the stability and control characteristics of whole TUAV are sensitive to the thickness of canard in transonic peed regime because of different canard vortex intensity and effect generated.

***Keywords*:** Unmanned air vehicle; Controlled canard; Aerodynamic characteristic; Wind tunnel test; Numerical simulation

1. Introduction

The target and training unmanned air vehicle (TUAV) is a dynamic simulator of the attacking object for various weapon systems. By now, multi-kinds of TUAV have been developed, of which the most famous ones are the "Chukar" series and the "Firebee" series etc [1]. The recent development of TUAV has the ability of modeling flight formation and high intelligence with low cost. A low-altitude high subsonic TUAV is being developed by our group. The TUAV works over an altitude range from 50~1000 m, with cruising speed between 0.7~0.85 Ma. The solid propellant rocket motor (SRM) is chosen as the power of such a TUAV. The advantage of using SRM is that its thrust is independent of cruising speed, altitude and environmental air, so it is easy to realize high subsonic cruise and high maneuver for the TUAV.

But for an SRM-based TUAV with long end-burning propellant placed in its chamber [2, 3], it probably has oversized centroid variation during work. This may not satisfy the request of the control system. There are two methods to solve the problem: using a long tail nozzle SRM with regular aerodynamic arrangement (see Fig. 1(a)), such as the classical French Exocet guided missile; or using the canard configuration arrangement with normal form SRM, such as the American Penguin anti-ship missile. By any of the two methods, the centroid of SRM-based TUAV can be conveniently adjusted to gain minimal variation when allocating components. But the canard arrangement will have more dischargeable capacity and less structure mass than the regular form for this type of TUAV, as shown in Fig. 1. The extra volume and

† This paper was recommended for publication in revised form by Associate Editor Kyongsu Yi

*Corresponding author. Tel.: +86 10 82339444, Fax.: +86 10 82339677
E-mail address: xk311531@126.com

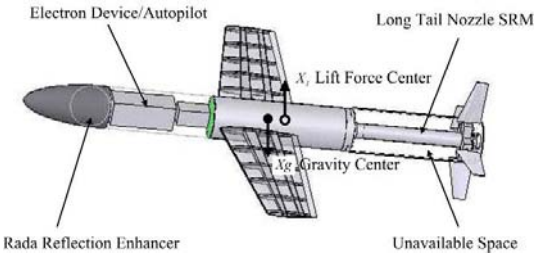

(a)

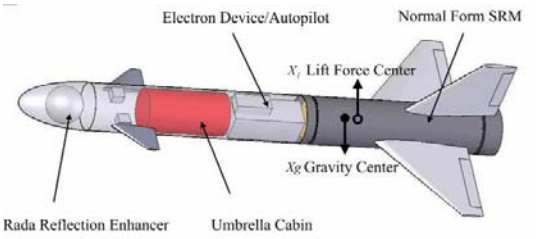

(b)

Fig. 1. The general arrangement of two design methods: (a) regular configuration, (b) canard configuration.

pay load enable it to impose an umbrella cabin additionally. This will make the SRM-based TUAV be reclaimed after work, which allows one to reduce cost.

Although controlled canard configuration has been considered to have quite excellent aerodynamic characteristics in longitudinal control, few cruise missiles or UAV apply such configuration in high subsonic speed regime. One of the probable reasons is that at nearly critical Mach number, the canard has complex interactions, as a function of angle of attack, with nose, body and tail wing, which may result in undesirable nonlinear control characteristics in this speed regime and make control system complicated. The interactions between canard and other elements are also hard to predict well in initial design. Although some corrected theoretical and semi-empirical methods developed by previous studies [4-7] can successfully predict canard-wing and canard-body interaction effect on static aerodynamic force and moment increment for some axisymmetric canard configurations, it has difficulty in expanding to predict some non-axisymmetric configurations and has to depend on specific experiment data at some speeds. Those methods also fail to predict the stability and control characteristics variation well when canard reflects, which is very important to the control system design.

Therefore, a controlled canard configuration concept for the TUAV was designed and studied in this paper. In the following, the wind tunnel experiment, semi-empirical method (DATCOM code) and the computational fluid dynamics (CFD) in the study will be viewed. Thereafter, the results will be discussed.

2. Methodology

The real object of the TUAV with a booster, two-stage combination, is shown in Fig. 2(a). The booster works for 1.6s, mainly to increase initial velocity of the TUAV, and the cruise SRM thruster works for 80s. When the booster finishes work, it is separated from the TUAV. The TUAV has a plane symmetry canard-body-multiple fin configuration. On the TUAV, canard is used as pitching control, following by the vertical tail and tail wings on which the yaw rudder and aileron is placed individually. Below the tail wing, there is a belly fin set. On the booster, four stabilizer fins are arranged as an ×- shaped pattern. The purpose for mounting belly fins is to increase yawing stability along with decreasing the rolling stability and forming a reflector with the tail wing to enhance the radar wave reflection at the tail. The nose outline is an oval shape.

The point G_1 in Fig. 2(a) is the reference point for aerodynamic moment. And the reference coordinate is shown in Fig. 2(b). The positive direction of aerodynamic force and moment is the same with the ref. coordinate. The directions of angle of attack α and angle of side slip β, shown in Fig. 2(b) individually, are positive. The sign definitions of angles of control surface are as follows: when aileron deflection angle δ_x is positive, negative rolling moment m_x is generated; when yaw rudder deflection angle δ_y is positive, negative yaw moment m_y is generated; when the canard deflection angle δ_z is positive, positive pitching moment m_z is generated.

The semi-empirical code DATCOM [8] was used to predict the aerodynamic force and moment at 0.7 and 0.8 Ma, for the initial configuration study and quick design. DATCOM has been widely used in projects for aerodynamic force and moment predictions of most air vehicle configurations [9-12]. The reference length and reference area values correspond to the mean chord of the tail wing and its plane area, respectively.

The numerical simulation of flow field was performed on the platform of FLUENT (v6.3). The structural grid was applied to mesh calculation region modeled in the GAMBIT (v2.3). To attain accurate

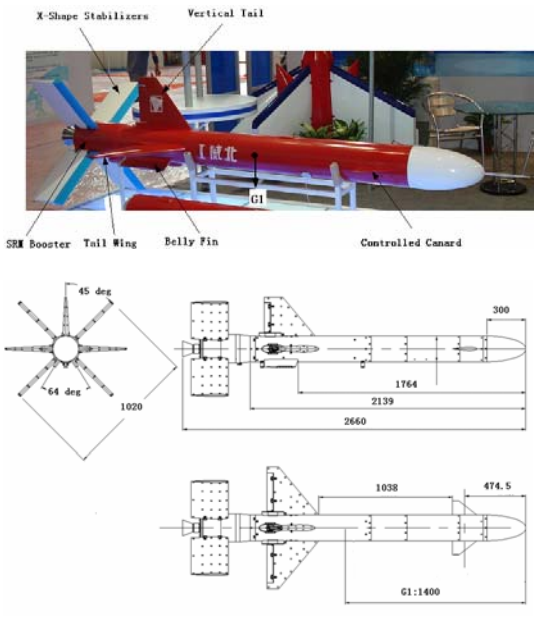

(a)

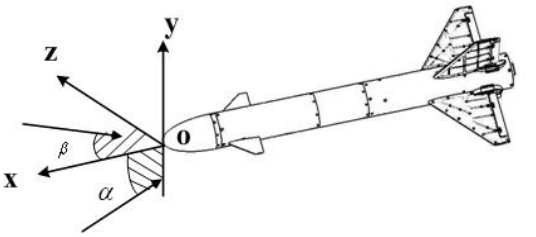

(b)

Fig. 2. Schematics of a) general dimension and b) reference coordinate.

CFD simulation result, the following details should be simulated carefully by CFD model: (1) the development of canard wake vortex in a transonic zone; (2) canard wake vortex interaction with tail wing; (3) multi element interactions and the influence of cross-flow on canard vortex track; and (4) transonic flow details on wing surfaces, such as local shocks and separation in boundary layer. The RANS equations were applied here to describe the turbulent flow. For practical engineering problems, different methods can be applied to resolve RANS equations for the mean flow quantities, with all the scales of the turbulence being modeled, such as Spalart-Allmaras [13-15], k-ε [16, 17], k-ω [18, 19] and their variants.

In this paper, the Spalart-Allmaras model was applied. The Spalart-Allmaras one-equation turbulence model has been demonstrated by some studies to be useful in accurately predicating flows about multi-element airfoils, high angles of attack, and airfoils where boundary-layer separation occurs [14]. The Spalart-Allmaras model has been modified to use in conjunction with the wall functions, for modeling the near-wall region. The mesh guidelines for the wall functions approach suggest that the distance from the wall at the wall-adjacent cell must be determined by considering the range of validity of the log-law. Because the log-law is valid for y^+>30 to 60, a value close to y^+=30 is recommended and the boundary layer should contain a few cells.

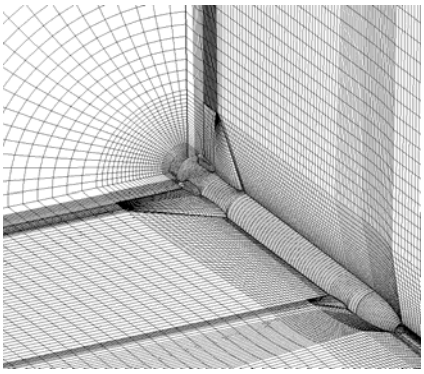

(a)

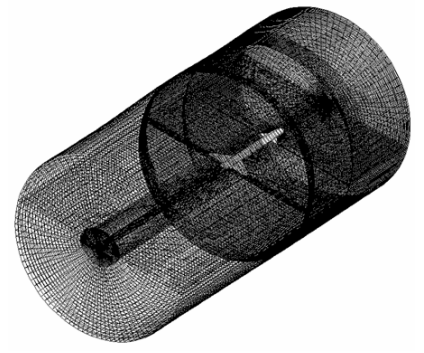

(b)

Fig. 3. Views of (a) structural mesh of calculation model and (b) entire calculation domain.

Second-order discretization schemes were employed and the convergence criterion was based on a four to five order-of-magnitude drop in the value of the residuals of mass, momentum, energy, and turbulent viscosity. Typical grids were on the order of 2.0 million cells. Grid adaptation basing on velocity gradient adaptation was used to increase the simulation accuracy and improve overall results. The calculation region and gird mesh is shown in Fig. 3.

3. Wind tunnel and test model

Experiments were conducted at the wind tunnel FD-08 of CAAA, Beijing, China [20]. FD-08 tunnel has a closed aerodynamic circuit with a Mach number range from Ma=0.3~1.3. The test section is rectangular and has dimensions of 0.76 m × 0.53 m and a length of 1.71 m. The upper and lower walls in the test section are open holes to reduce background noise, with ΔC_p<0.05 for the balance measurements. ΔC_p is pressure coefficient error.

In the tests, the Mach number of modeled free stream was kept constant within ±0.005 Ma. The temperature of the air was constant at a value of T=296 K within ±1%, and the atmospheric pressure P=1.01×105 Pa within ±2%. The test conditions for the current investigation covered a range of angle of attack from -8 deg to 12 deg within ±0.05 deg, and a range of Mach numbers from 0.3 to 0.8 Ma which gives a range of chord Reynolds numbers from 1.54×10^6 to 3.31×10^6 based on model mean chord.

The fully equipped wind tunnel model was developed and built to a scale of 1:4.5 at CAAA. The control surface of the model can be reflected (canard:-15 deg ~ 15 deg, aileron: -20 deg ~ 20 deg, yaw rudder: -20 deg ~ 20 deg). The model mounted on a holder in the wind tunnel is displayed in Fig. 4. In the tests, the basic static force and moment experiments and the control efficiency experiments are all included.

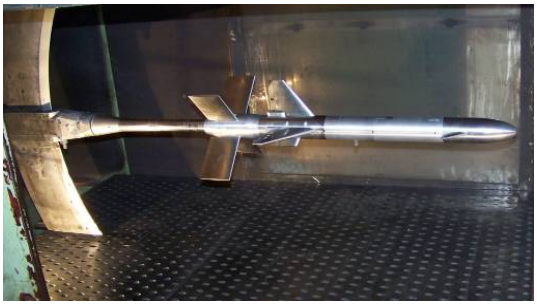

(a)

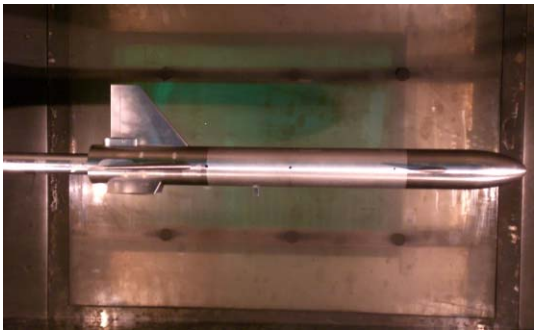

(b)

Fig. 4. Wind tunnel test models of (a) two-stage combination of TUAV and booster, and (b) single TUAV, mounted in wind tunnel FD-08.

4. Results and discussion

4.1 Preliminary configuration

The aerofoil initially used and parameters of platform are listed in Table 1. In this section, the longitudinal aerodynamic characteristic will be focused on for discussion. The comparison of pitching moment and force coefficients between DATCOM and experimental results is given in Fig. 5(a), (b), and the test results of single TUAV without canard and two-stage combination with controlled canard are shown in Fig. 5(c), (d) individually.

The experiment data in Fig. 5(a) and (b) show that the preliminary configuration of TUAV has large negative pitching moment and nonzero lift force coefficient at zero angle of attack (m_{z0} and C_{y0}), because of a non-axisymmetric configuration type. However, the perdition value of m_{z0} by DATCOM is zero. It illustrates that DATCOM has difficulty in predicting m_{z0} for such a non-axisymmetric canard configuration type. In fact, the reason for creating minus m_{z0} and nonzero C_{y0} is the unbalanced pressure distribution between the upside and downside walls of fuselage, near the vertical tail and the belly fins. As shown in Fig. 5(a), DATCOM can only follow the trend of wind tunnel data, but overestimates the stability over the entire angle-of-attack range at Mach numbers 0.7 and 0.8 with large error. It is noticed that, at

Table 1. Key features of wings.

	Airfoil	Semi wing span (mm)	Leading-edge sweep angle (/ º)	Root chord (mm)
Canard	NACA 0012	117.5	50	187.5
Tail wing	NACA 0012	372	40	403.5
Vertical tail	NACA 0010	300	40	394.4
Belly fin	NACA 0009	65	20	265
Stabilizer	NACA 0009	400	0	290

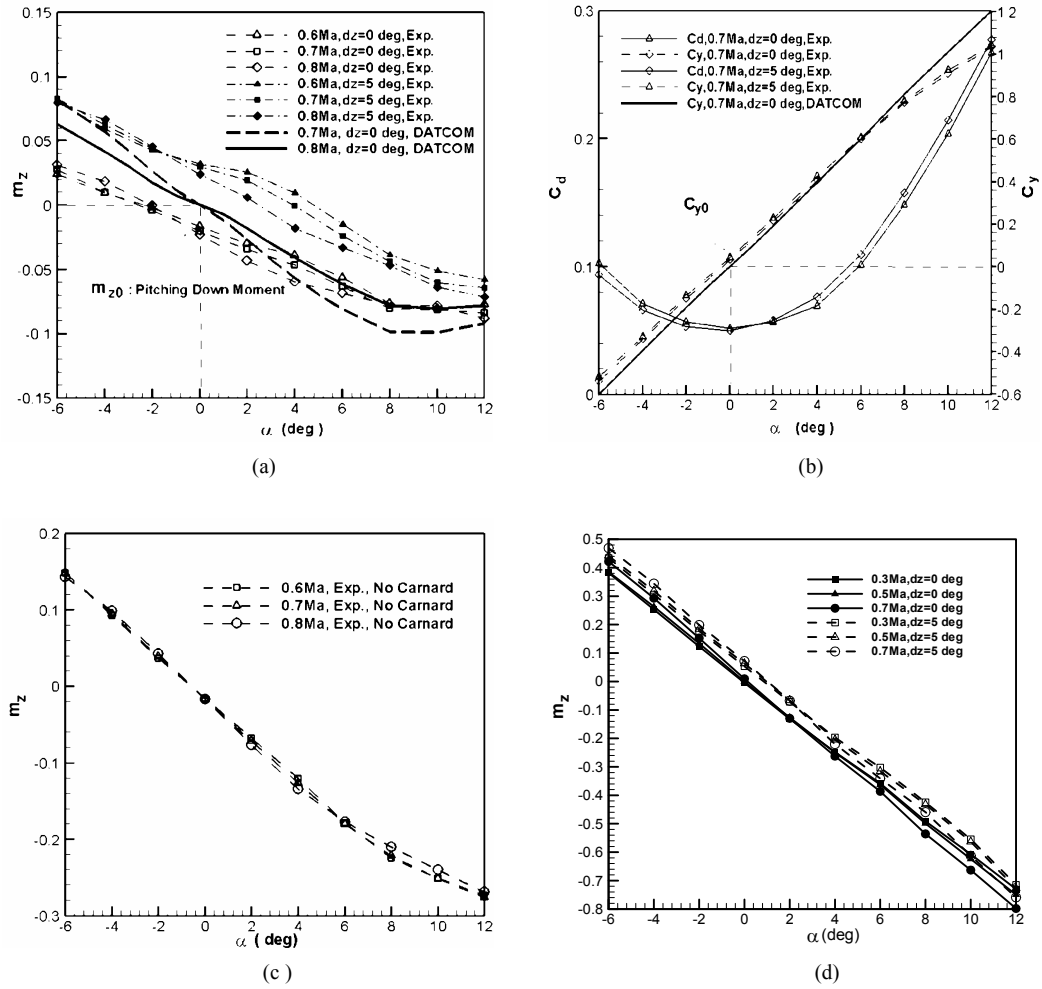

Fig. 5. Wind tunnel test results: (a) pitching moment coefficients vs. α for single TUAV, (b) lift and drag coefficients vs. α for single TUAV, (c) pitching moment coefficients vs. α for single TUAV without canard, and (d) pitching moment coefficients vs. α for the two-stage combination, β=0 deg.

angles of attack from -6 to 8 deg, DATCOM can produce reasonable lift force derivative compared with experimental data.

In Fig. 5(c), without canard interfaces, the variation of pitching moment coefficients with angle of attack is reasonably linear over an angle-of-attack range from -6 to 8 deg, at Mach numbers 0.6, 0.7, and 0.8. The configuration is stable with almost the same stability in the test conditions. After adding canard (see Fig. 5(a)), the variation of pitching moment coefficients with angle of attack shows a nonlinear trend. With respect to the conditions of removing the canard, the stability of whole TUAV is varying with Mach numbers at the same given angle of attack. The stability of TUAV decreases at low angles of attack between 0 and 4 deg as Mach number increases, and get closely to neutral stable when the canard reflects 5 deg. The comparison of the two tests proves the interfaces between canard and the other elements have strong nonlinear effects. The nonlinear effect is undesirable for the TUAV here. It will increase difficulty and cost for the control system.

Negative m_{z0} and insufficient stability are also unfavorable to control for such a TUAV. Especially when the booster departs, there will be large disturbance, which probably results in losing control of flight. Therefore, the configuration concept was improved to decrease canard nonlinear interactions and pitching moment at zero angle of attack, and to improve stability quality when canard reflects. Since

DATCOM cannot predict well m_{z0} and m_z for such a canard configuration type, the CFD method is applied to learn nonlinear canard-element interactions in detail for further study and improving design.

In Fig. 5(d), it is interesting to note that the m_{z0} of two-stage combination in tests turns to zero. That is, because after adding a booster, the main lift surface of the whole flying vehicle turns to the axisymmetric ×-shaped stabilizer fins. When free-stream air flows past them, the pressure distribution of the vehicle tends to be axisymmetric. Besides, the ×-shaped stabilizer fins have a biased 45 deg with tail wing and canard of the TUAV in circumferential direction. Hence, the stabilizer fins are little influenced by wake flow of front wings. It results in a linear trend for variation of pitching moment coefficients with angle of attack, even if the canard reflects. The tests also show another advantage of controlled canard arrangement in that the canard can be used to control pitching movement of the two-stage combination in the launch stage before the booster departs from TUAV.

An external flow field simulation was conducted over a range of angle of attack from -4 to 8 deg (2 deg interval), at Mach numbers 0.6, 0.7, and 0.8. The pitching moment coefficients predicted by CFD show good agreement with the test results, as shown in Fig. 6. Only up to 8 deg angle of attack, can an obvious difference between them be observed with the maximum error about 12%. Since the frequently used angle of attack for the TUAV is between -6 deg and 6 deg, the calculation can be considered to have good accuracy and be able to aid in improving design.

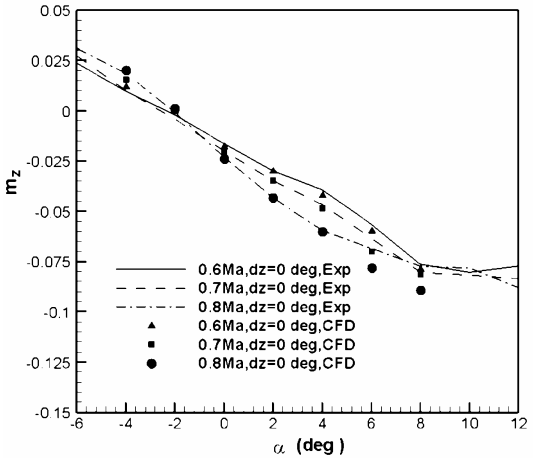

Fig. 6. Comparison of pitching moment coefficient for single TUAV between wind tunnel tests and CFD estimation.

The Mach contours and plots on the surfaces of tail wing and canard at 0.8 Ma are shown in Fig. 7(a). It is observed that as angle of attack increases the maximum Mach number on wing surfaces increases from 0.98 to 1.55. The surface near wing tip experiences transonic flow when angle of attack increases from 0 deg up to 8 deg. It can be expected that a similar situation is experienced on the surface of the canard when the canard defection angle increases.

The streamlines from the surface of the canard and tail wing are shown in Fig. 7(b), at Mach number 0.8 with angle of attack 2 deg. From front view, the stereo structure of wake vortex developed from tail edge of wings can be observed. Canard wake vortex trajectories in the flow field show that the canard vortex core travels through the transonic region (see Fig. 7(a)) on the tail wing. The parameters in transonic zone are unstable, and have large disturbance when the canard vortex goes through it.

Fig. 7(c) shows that, at low angles of attack, the canard vortex gets quite close to the surface of tail wing, and the velocity component induced by the canard vortex changes the local transonic flow condition. The wake vortex intensity will increase if the canard reflects, and will strengthen the influence on static pressure distribution of the tail wing. As angle of attack increases, vortex trajectory tends to leave away local transonic flow zone of the tail wing surface, which makes the interaction between canard vortex and tail wing become weak. It can explain why the pitching moment coefficients vs. angle of attack curve shows nonlinear as a function of angle of attack and fight Mach numbers. Fig. 7(d) gives the velocity vectors of cross flow at x=-1.9 m. It indicates that there exist complicated interfaces and cross flow between multi elements. The canard vortex trajectory is also affected by the cross-flow, which makes the canard-tail wing interaction more complicated.

Fig. 7(e) gives the pressure distribution on the upside and downside walls of the fuselage along two lines, which are symmetric with the central plane (y=±0.05 m, see Fig. 7(c)). It is observed that since from x=-1 m, there exists an obvious difference for pressure distribution on the fuselage. That is the reason for generating large negative pitching moment at zero angle of attack for the initial TUAV configuration concept.

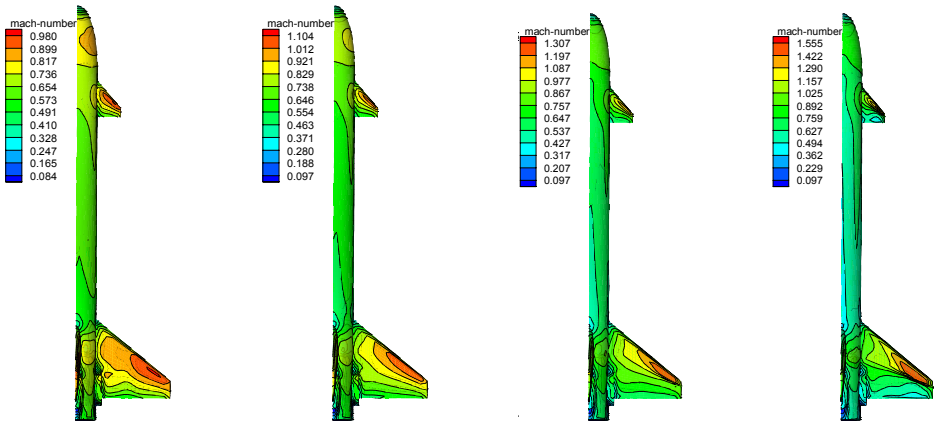

α=0 deg, Ma_∞=0.8 α=2 deg, Ma_∞=0.8 α=4 deg, Ma_∞=0.8 α=8 deg, Ma_∞=0.8

(a)

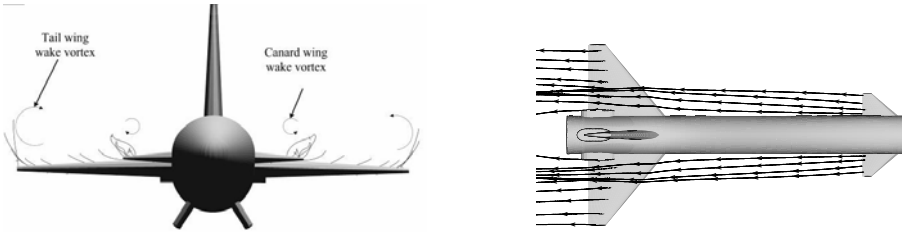

Front view Top view

(b)

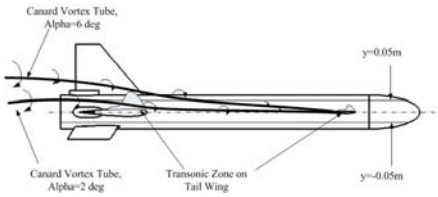

(c)

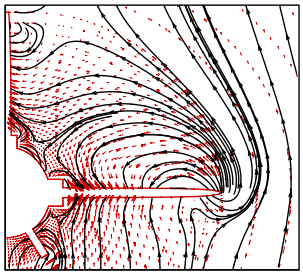

(d)

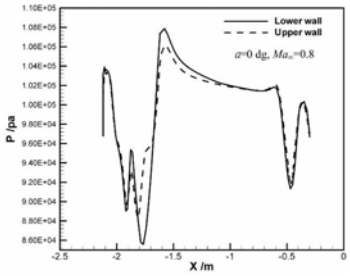

(e)

Fig. 7. CFD simulation results: (a) Mach contours and plots, Ma_∞=0.8, (b) stream lines on canard and tail wing, at α=2 deg, Ma_∞=0.8, (c) canard vortexes track, (d) velocity vectors, at x=-1.9m, α=2 deg, Ma_∞=0.8, and (e) pressure distribution on the fuselage along two lines at y=±0.05m.

4.2 Improved configuration

Under the guidance of CFD simulation, the final improved parameters are summarized in Table 2. Based on CFD simulation, the airfoil of vertical tail is changed to NACA0008, and the belly fin is lengthened. The aim of those changes is to slow down the velocity along the upside wall and accelerate the velocity along the downside wall to balance pressure distribution of the fuselage. The airfoil of the canard was changed to NACA0007, but the tail wing was unchanged.

The pitching moment coefficient results of wind tunnel tests and CFD for final improved configuration are presented together in Fig. 8(a). The CFD results still agree well with the test data. The m_{z0} of new configuration gets close to zero. The variation of pitching moment coefficients with angles of attack tends to show a closely linear law at angles of attack from -4 to 8 deg. And the nonlinear effect deduced by canard deflection is decreased considerably but with almost the same control pitching moment increment Δm_z (δ_z =5 deg) as the unimproved one. It is emphasized that the improved TUAV has a better longitudinal stability quality only by decreasing the thickness of canard without changing tail wing parameters. Fig. 8(b) reveals that the improved configuration has slight reduction in lift coefficient with friction drag coefficient almost unchanged. But when the canard has 5 deg of reflection, the total drag coefficient of the improved configuration is smaller than the unimproved one. It illustrates that NACA0007 canard causes less induced drag for the TUAV when it reflects.

Fig. 9 shows the chordwise pressure coefficients by CFD on tail wing surface for the three configuration conditions of adding canard (NACA0012 and NACA0007 canard) and removing canard, at angles of attack 2, 4 deg of 0.8 Ma. The results reveal how the canard wake vortex influences pressure distribution on tail wing surface when it trails through the transonic zone. The downside chordwise pressure coefficients at the two spanwise places (z=0.22 m, and z=0.4 m) are almost the same between the three configuration conditions at positive angle of attack. It indicates that the canard wake flow only influences the upside pressure distribution of tail wing at positive angle of attack.

Fig. 9(a) and (b) give chordwise pressure coefficients at spanwise place of z=0.22 m, where the canard wake vortex core trails through (see Fig. 6(b), top view). At low angle of attack, the NACA 0012 canard vortex flow mainly results in the increment of static pressure at the leading edge up to 10% local chord, compared with the same condition of NACA0007 (Fig. 9(a)). As angle of attack increases, the canard vortex influence zone on the tail wing tends to move downstream by comparing Fig. 9(a) and (b). And the difference of chordwise pressure

Table 2. Parameters for the improved wings.

	Airfoil	Semi wing span (mm)	Leading-edge sweep (/°)	Root chord (mm)
Canard wing	NACA 0007	Unchanged	Unchanged	Unchanged
Vertical tail	NACA 0008	Unchanged	Unchanged	Unchanged
Belly fin	Unchanged	65	20	370

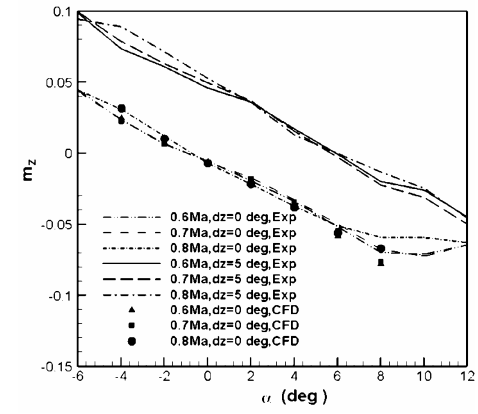

(a)

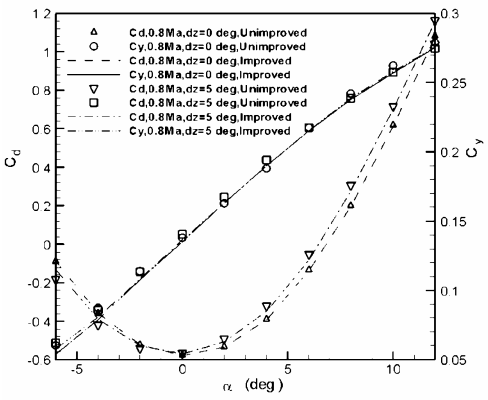

(b)

Fig. 8. Results for the improved configuration: (a) comparison of pitching moment coefficient between wind tunnel tests and CFD estimation, and (b) comparison of lift and drag coefficients between unimproved and improved configurations.

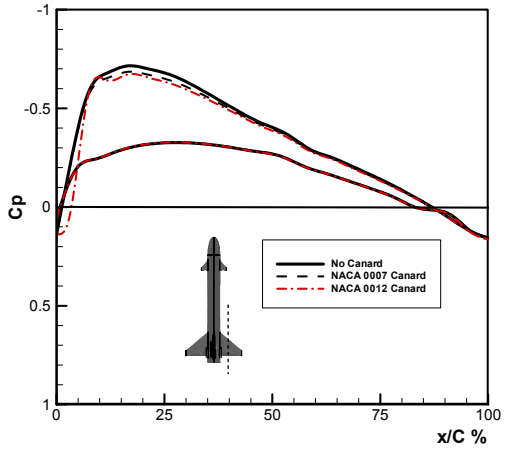

(a) z=0.22 m, α=2 deg, β=0 deg

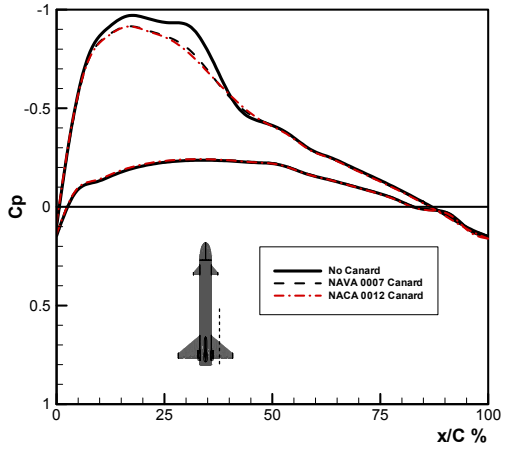

(b) z=0.22 m, α=4 deg, β=0 deg

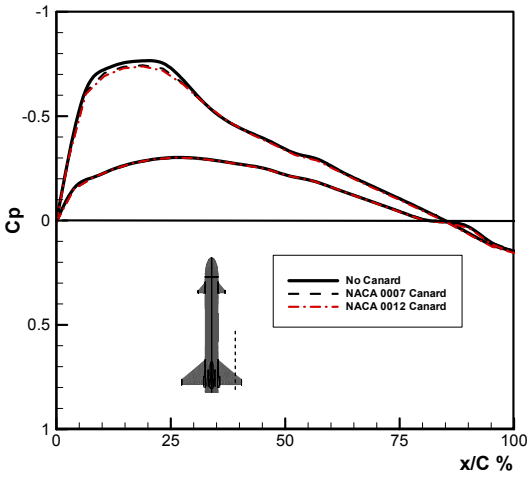

(c) z=0.4 m, α=2 deg, β=0 deg

Fig. 9. Chordwise pressure coefficient distribution at spanwise places of z=0.22 m and z=0.4.

coefficients between the conditions of NACA0012 and NACA0007 becomes small. That is because the canard vortex is closest to the tail wing and the influence is strongest at a small angle of attack. When the angle of attack increases, the canard vortex tube gradually leaves away from the surface of the tail wing (see Fig. 6(c)), and the influence of vortex intensity gets weak. Therefore, a thick canard with stronger vortex intensity tends to show an obvious nonlinear characteristic in pitching moment coefficient vs. angle of attack curve, compared with the thin canard at low angles of attack.

Fig. 9(c) gives the chordwise pressure coefficients at spanwise place of z=0.4 m, where the flow zone is out of canard vortex core. At this place, the two configurations with NACA0012 canard and NACA0007 canard tend to have the same chordwise pressure coefficient distribution. And the difference between the configurations of adding canard and removing canard is small, because it is less interfaced by canard vortex core than the position at z=0.22 m.

5. Conclusions

The controlled canard configuration of an SRM-based TUAV has been designed and improved in this paper, with cruise Mach numbers between 0.7-0.85. The semi-empirical code DATACOM, CFD and wind tunnel test were used to study its aerodynamic characteristics. Compared to the test results in high subsonic flight conditions, DATCOM shows difficulty in predicting the integrated nonlinear effect of canard-element interactions on stability and control characteristics for the researched configuration type. The CFD model built by this paper produces accurate aerodynamic force and moment coefficients at frequently used angles of attack. Hence the CFD method is used in guiding design improvement to save experimental cost.

Both CFD and wind tunnel tests show that, in transonic speed regime, the macroscopic stability and control characteristic of whole TUAV mainly depending on canard vortex behavior and interactions with tail wing, shows sensitivity to the thickness of the canard. At small angle of attack, the canard vortex is closest to the tail wing and influences its static pressure distribution at the leading edge. When the angle of attack increases, the canard vortex leaves the tail wing surface, and the vortex core disturbance becomes weak. Therefore, when a thick canard with strong vortex intensity is imposed, the TUAV shows

strongly undesirable nonlinear stability characteristic. Using a thin controlled canard can decrease the undesirable nonlinear canard-element interactions and improve the stability quality, especially when the canard reflects for the TUAV.

The experimental and simulation results presented by this paper can also be used to expand and implement the design database or to examine the other semi-empirical methods of aerodynamic coefficient prediction for similar non-axisymmetric controlled canard configuration.

Acknowledgment

This work was financially supported by Beijing University of Aeronautics and Astronautics. The author would also like to thank the support of China Academy of Aerospace Aerodynamics for their help in the wind tunnel experiments.

References

[1] D. A. Fulghum, Targets Become UAVs, *Aviation Week and Space Technology,* 159 (4) (2003) 54-55.

[2] J. L. Quilici, Nozzle Development for the Proposed AGM-130 Rocket Motor, *AIAA Paper* 84-1415.

[3] B. M. Dunn, M. R. Durbin and A. L. Jones et al., Short Range Attack Missile (SRAM) Propulsion, 3 Decades History, *AIAA Paper* 94-3059.

[4] F. G. Moore, T. Hymer and R. Mclnville, A Planar Nonlinear Missile Aeroprediction Code for All Mach Numbers, *AIAA Paper* 94-0026.

[5] M. G. Landers, L. H. Hall and L. M. Auman, Aerodynamic Predictions of Pitch and Roll Control for Canard-Controlled Missiles, *AIAA Paper* 2000-4516.

[6] Y. Guy, T. E. McLaughlin and J. R. Morrow, Effects of Canard Shape on the Center of Pressure of a Generic Missile Configuration, *AIAA Paper* 2000-0026.

[7] A. Sigal, Interactions between a Canard and Thick Bodies: Analysis and Applications, *Journal of Aircraft*, 38 (6) (2001) 888-896.

[8] Public Domain Aeronautical Software, USAF Stability and Control Datcom, Updated St. Luis Div., Santa Cruz, CA, 1999. URL: http://instructional1.calstatela.edu/cwu/me454/DatCom/DLLs/.

[9] T. J. Sooy and R. J. Schmidt, Aerodynamic Predictions, Comparisons, and Validations Using Missile Datcom (97) and Aeroprediction 98 (AP98), *Journal of Spacecraft and Rockets*, 42 (2) (2005) 257-265.

[10] T. Wagner and J. Valasek, Comparison of Computational Methods for Stability and Control Analysis, *AIAA Paper* 2005-140.

[11] S. Shivananda, S. Mckeel and M. Salita et al., Space Launch Vehicle Aerodynamics Comparison of Engineering and CFD Predictions with Wind Tunnel Data, *AIAA Paper* 2001-0258.

[12] S. R. Vukelich and J. E. Williams, The USAF Stability and Control Digital Datcom, AFFDL-TR-81-30 (1982).

[13] M. Rudman, One-Equation Turbulence Model For Generalized Newtonian Fluid Flow, Thesis, William Marsh Rice University, Houston, TX, (2003).

[14] J. Pan, E. Loth and M. B. Bragg, RANS Simulation of Aerofoils with Ice Shapes, *AIAA Paper* 2003-0729.

[15] P. Sparlart and S. Allmaras, A One-equation Turbulence Model for Aerodynamic Flows, *AIAA Paper* 92-0439.

[16] B. E. Launder and D. B. Spalding, Lectures in Mathematical Models of Turbulence, Academic Press, London, (1972).

[17] V. Yakhot and S. A. Orszag, Renormalization Group Analysis of Turbulence, 1: Basic Theory, *Journal of Scientific Computing*, 1 (1) (1986) 3-51.

[18] F. R. Menter, Improved Two-Equation k-omega Turbulence Models for Aerodynamic Flows, NASA TM 103975, (1992).

[19] F. R. Menter, Two-Equation Eddy-Viscosity Turbulence Models for Engineering Applications, *AIAA Journal*, 40 (2) (2003) 290-296.

[20] J. C. Fan, Handbook of Wind Tunnel Test, Aeronautic Industry Press, Bei Jing, PRC, (2002). [in Chinese].

[21] F. A. Khan and T. J. Mueller, Tip Vortex/Aerofoil Interaction for a Canard/Wing Configuration at Low Reynolds Numbers, *AIAA Paper* 89-0536.

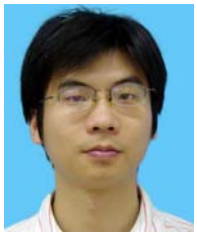

XIE Kan received his B.S. degree from Beijing University of Aeronautics and Astronautics, China, in 2005, and then was recommended as a Ph.D. candidate there. His main research interest is aerodynamic design of Unmanned Air Vehicles.